Journal of Power Sources 209 (2012) 52–56

Contents lists available at SciVerse ScienceDirect

Journal of Power Sources

journal homepage: www.elsevier.com/locate/jpowsour

Short communication

Intermediate-temperature ionic liquid NaFSA-KFSA and its application to sodium secondary batteries

Atsushi Fukunaga[a,b], Toshiyuki Nohira[a,*], Yu Kozawa[a], Rika Hagiwara[a,*], Shoichiro Sakai[b], Koji Nitta[b], Shinji Inazawa[b]

[a] Graduate School of Energy Science, Kyoto University, Sakyo-ku, Kyoto 606-8501, Japan
[b] Electronics & Materials R&D Laboratories, Sumitomo Electric Industries, Ltd., Konohana-ku, Osaka 554-0024, Japan

ARTICLE INFO

Article history:
Received 26 January 2012
Accepted 16 February 2012
Available online 25 February 2012

Keywords:
Sodium secondary battery
Intermediate temperature
Ionic liquid
Bis(fluorosulfonyl)amide
$NaCrO_2$

ABSTRACT

The physicochemical properties of an intermediate-temperature ionic liquid (ITIL), NaFSA-KFSA ($x_{NaFSA} = 0.56$, $x_{KFSA} = 0.44$, and FSA = bis(fluorosulfonyl)amide), were investigated to test the potential of the ITIL as an electrolyte for sodium secondary batteries operating at intermediate temperatures (333–393 K). The viscosity, ionic conductivity, and density of this ITIL, measured at 363 K, were 435 cP, 3.3 mS cm^{-1}, and 2.14 g cm^{-3}, respectively. Cyclic voltammetry revealed that the electrochemical window is as wide as 5.2 V at 363 K, and that reversible electrochemical deposition/dissolution of sodium metal occurs at the cathode limit potential. A Na/NaFSA-KFSA/$NaCrO_2$ cell was constructed and its charge–discharge properties investigated at 353 K. The discharge capacity at the 1st cycle was 77.3 mA h $(g\text{-}NaCrO_2)^{-1}$ at 15 mA $(g\text{-}NaCrO_2)^{-1}$. Except for the initial few cycles, the coulombic efficiencies were higher than 99.9% for 100 cycles, and 89% of the initial discharge capacity was maintained after 100 cycles. Considering its non-volatility, non-flammability, and low cost, this inorganic ITIL is highly promising as a new class of electrolyte for sodium secondary batteries.

1. Introduction

In order to introduce renewable energy technologies, such as photovoltaics and wind power generators, the development of inexpensive and efficient power storage devices is essential. One approach for this is the scale-up of lithium ion batteries [1,2]. However, in order to realize the widespread use of large-scale batteries throughout the world, it is clear that current lithium ion batteries have several crucial problems. One problem is the use of rare metals such as cobalt as materials for the positive electrode. Even if this problem has been resolved through the introduction of iron-based materials, retaining a stable and low-priced supply of lithium itself may be difficult in the future. Another problem is the use of volatile, flammable, and expensive organic electrolytes, which is a significant disadvantage in realizing safe and inexpensive batteries. In addition, the thermal instability of current lithium ion batteries, which results from the use of organic electrolytes, hinders the realization of large-scale batteries possessing high energy and power density because the cells cannot be packed close together. This in turn means that temperature elevation cannot be utilized to enhance the reaction and mass transfer.

To overcome the inherent problems of lithium ion batteries, sodium secondary batteries are attracting much attention as one form of post-lithium ion battery [3–10]. Historically, Na/S batteries [11,12] and Na/$NiCl_2$ batteries [13,14] have been studied for almost 30 years. They have already been partly applied in practice. In both batteries, β″-alumina ($Na_2O{\cdot}xAl_2O_3$, $5 \leq x \leq 7$) is used as a solid electrolyte, with operating temperatures as high as approximately 573 K in order to ensure sufficient ionic conductivity of sodium ion. Therefore, heaters and heat insulators are required to maintain the operating temperature, which leads to an increase in size and weight of the batteries. Moreover, consumption of energy by the heaters reduces the energy density of the total battery system. There is also the danger of a serious accident occurring through an electrical short circuit if the mechanically fragile β″-alumina breaks during the operation because in this temperature region sodium is in the liquid state and highly reactive. Thus, it is important to develop sodium secondary batteries that do not use β″-alumina and that can operate at lower temperatures. However, most of the reported sodium secondary batteries operating at room temperature have been constructed using organic electrolytes such as $NaClO_4$/propylene carbonate [3–9]. Since these are volatile and flammable, these batteries encounter the same problems as do current lithium ion batteries in scaling up. Thus, the development

* Corresponding authors. Tel.: +81 75 753 5822; fax: +81 75 753 5906.
E-mail addresses: nohira@energy.kyoto-u.ac.jp (T. Nohira), hagiwara@energy.kyoto-u.ac.jp (R. Hagiwara).

0378-7753/$ – see front matter © 2012 Elsevier B.V. All rights reserved.
doi:10.1016/j.jpowsour.2012.02.058

of new batteries with improved safety and better performance is strongly required.

Ionic liquids have been studied as safe electrolytes for lithium ion batteries because they generally provide negligibly low volatility, nonflammability, and high thermal and electrochemical stability. More particularly, intense interest has been shown towards room-temperature ionic liquids (RTILs) over the past decade. However, low ionic conductivity, high viscosity and, in some cases, high cost has perhaps prevented RTILs from being of practical use. It is our claim that there are many advantages to the use of molten salts (or ionic liquids in original definition [15,16]) at intermediate temperatures (e.g., 373–473 K) [17]. Their advantages are remarkable when they are used as electrolytes for large-scale lithium [18] and sodium [19,20] secondary batteries, including improved ionic conductivity, decreased viscosity, enhanced reaction rate, the possibility of new electrode active materials, a simplified cooling system, and the efficient use of generated heat.

We first focused on salts consisting of alkali metal cations and the bis(trifluoromethylsulfonyl)amide (TFSA) anion, MTFSAs (M = Li, Na, K, Rb, or Cs), and reported that they have melting points in the range of 400–540 K. These melting points are significantly lowered by mixing two or three of these salts in prescribed compositions [21,22]. Such mixed salts of MTFSA possess wide electrochemical windows of approximately 5 V [23]. We have reported that the LiTFSA-KTFSA-CsTFSA system shows promise as an electrolyte for lithium metal secondary batteries, and that a Li/$LiFePO_4$ cell exhibits good cycle performance at 423 K [18]. Recently, we also reported that a Na/NaTFSA-CsTFSA/$NaCrO_2$ cell shows promise as a sodium secondary battery that can operate at around 423 K [19]. Furthermore, in order to develop salts with lower melting points, we investigated MFSA ionic liquids that consist of alkali metal cations and bis(fluorosulfonyl)amide (FSA) anion, and found that binary and ternary MFSAs (M = Li, Na, K, Rb, or Cs) mixtures possess lower melting points than those of the single constituent salts [24–27]. Table 1 shows the eutectic compositions and temperatures of binary MFSA salt mixtures [26]. Although the melting points of single MFSA salts are relatively high (typically above 370 K), it is possible to lower the melting points to around 330 K through mixing. We pointed out that the NaFSA-KFSA system is expected to operate as an electrolyte for a sodium secondary battery at 353 K [24]. It should be noted that both NaFSA and KFSA are completely inorganic compounds and as such are expected to be synthesized with a reasonably low cost because they do not contain expensive organic cations. Furthermore, FSA anions can be synthesized without using the expensive electrofluorination process.

In the present study, we measured the viscosity, ionic conductivity, and density of a NaFSA-KFSA eutectic melt (x_{NaFSA} = 0.56 and x_{KFSA} = 0.44) at 333–398 K since these are the fundamental electrolyte properties for use in a sodium secondary battery. The relationship between viscosity and molar conductivity was discussed from the Walden plot. The electrochemical window of the melt was investigated to reveal its accessible potential range. The stability of aluminum, which is used as a current collector of the positive electrode, was also studied. Finally, a Na/NaFSA-KFSA/$NaCrO_2$ cell was constructed and its charge–discharge properties investigated at 353 K. Here in, $NaCrO_2$ was selected as a positive electrode active material because it had previously been reported to exhibit good cycle performance at both room [7] and high temperature [19].

Table 1
The eutectic temperatures and compositions of binary MFSA (M = Li, Na, K, Rb, Cs) systems [26].

System	x_{MFSA}	T_m (K)
LiFSA-NaFSA	*E*: x_{LiFSA} = 0.40, x_{NaFSA} = 0.60	349
LiFSA-KFSA	*E*: x_{LiFSA} = 0.41, x_{KFSA} = 0.59	341
LiFSA-RbFSA	*E*: x_{LiFSA} = 0.38, x_{RbFSA} = 0.62	337
LiFSA-CsFSA	*E*: x_{LiFSA} = 0.47, x_{CsFSA} = 0.53	335
NaFSA-KFSA	*E*: x_{NaFSA} = 0.56, x_{KFSA} = 0.44	334
NaFSA-RbFSA	*E*: x_{NaFSA} = 0.50, x_{RbFSA} = 0.50	328
NaFSA-CsFSA	*E*: x_{NaFSA} = 0.47, x_{CsFSA} = 0.53	325
KFSA-RbFSA	*E*: x_{KFSA} = 0.31, x_{RbFSA} = 0.69	354
KFSA-CsFSA	*E*: x_{KFSA} = 0.54, x_{CsFSA} = 0.46	336
RbFSA-CsFSA	*E*: x_{RbFSA} = 0.65, x_{CsFSA} = 0.35	360

2. Experimental

NaFSA and KFSA (Mitsubishi Materials Electronic Chemicals, purity >99.0%) were purchased and dried under vacuum at 330 K for 24 h. Then, they were mixed into a eutectic composition (x_{NaFSA} = 0.56 and x_{KFSA} = 0.44). Density was measured using the Archimedes method by measuring the weight change of a volume-known nickel ball immersed in the melt. Viscosity was measured by a viscometer (Brookfield Engineering Laboratories, DV-II+ PRO). Ionic conductivity was measured by electrochemical impedance spectroscopy using a calibrated cell with two platinum plate electrodes and a potentiostat/galvanostat/frequency response analyzer (Ivium Technologies, IviumStat). The cell constant was determined with a standard KCl aqueous solution. The density, viscosity, and ionic conductivity were measured from 333 K to 398 K at intervals of 5 K.

Electrochemical measurements were performed with a three-electrode system constructed in a Pyrex® beaker cell in an argon-filled glove box. The electrochemical window of the eutectic NaFSA-KFSA melt was measured by cyclic voltammetry. A copper plate disk (6 mm in diameter and 0.1 mm in thickness) and a glassy carbon disk (3 mm in diameter) were used as working electrodes to investigate the cathode and anode limits, respectively. Sodium foils were used for counter and reference electrodes. The scan rate for the cyclic voltammetry was 10 mV s^{-1}. Galvanostatic electrolysis was performed to obtain the deposit for the identification of the reactions at the cathode limit. The deposited substance was analyzed by means of differential scanning calorimetry (DSC) and X-ray diffraction (XRD) analysis. The stability of aluminum was investigated by cyclic voltammetry and potentiostatic electrolysis. An aluminum plate (15 mm in diameter and 0.1 mm in thickness) was used as a working electrode.

The charge–discharge property of the Na/NaFSA-KFSA/$NaCrO_2$ cell was measured by a two-electrode cell. The positive electrode active material, $NaCrO_2$, was prepared by a solid phase method. Equimolar Na_2CO_3 and Cr_2O_3 were mixed and then reacted at 1123 K for 5 h under Ar flow. The $NaCrO_2$ thus prepared was well mixed with acetylene black (Wako Pure Chemical Industries, purity >99.99%) and PTFE (Sigma–Aldrich) at a weight ratio of 85/10/5 using a mortar and pestle. The resultant mixture was then pressed onto an aluminum mesh current collector at 300 MPa. Sodium foil was used as a negative electrode. A glass fiber filter paper (200 μm in thickness) was used as a separator. Charge–discharge tests were conducted at a constant current rate of 15–150 mA (g-$NaCrO_2$)$^{-1}$. All measurements were conducted in an argon glove box with a gas-refining instrument. The cell temperature, 353 K, was controlled by a heater with a temperature controller.

3. Results and discussion

3.1. Physicochemical properties of the eutectic NaFSA-KFSA melt at 333–398 K

Fig. 1 shows an Arrhenius plot of viscosity for the eutectic NaFSA-KFSA melt. The viscosity was 435 cP at 363 K. Distinct upward trends in the curvatures are observed at lower

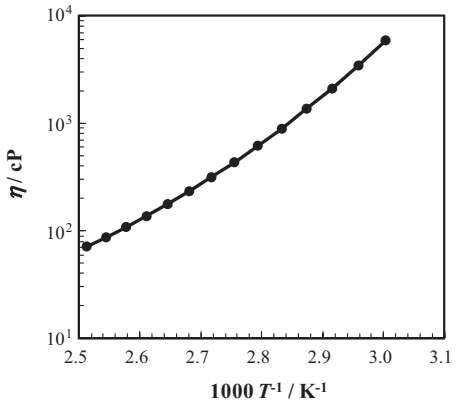

Fig. 1. Arrhenius plot of viscosity for a NaFSA-KFSA eutectic melt.

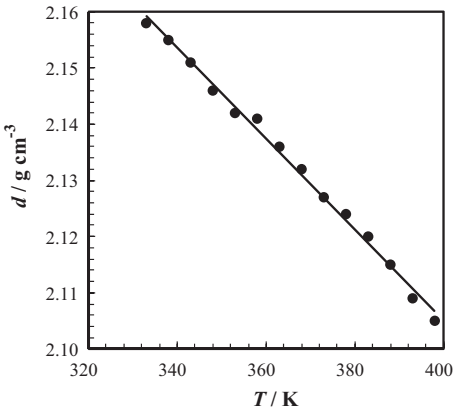

Fig. 3. Temperature dependence of density for a NaFSA-KFSA eutectic melt.

temperatures. In such a case, the following Vogel–Tamman–Fulcher (VTF) equation [28] is frequently applied:

$$\eta(T) = A_\eta \sqrt{T} \exp\left(\frac{B_\eta}{T - T_{0\eta}}\right), \quad (1)$$

where A_η, B_η, and $T_{0\eta}$ are constants that are determined empirically. $T_{0\eta}$ is called the "ideal glass transition temperature." The viscosity of the NaFSA-KFSA melt fitted well ($R^2 > 0.999$) to the VTF equation with $A_\eta = 3.87 \times 10^{-3}$ cP $K^{-1/2}$, $B_\eta = 1111$ K, and $T_{0\eta} = 235$ K.

Fig. 2 shows an Arrhenius plot of ionic conductivity for the eutectic NaFSA-KFSA melt. The conductivity was measured as 3.3 mS cm^{-1} at 363 K. Slightly downward curvatures are observed at lower temperatures. Similarly to the case of viscosity, such temperature dependence is described by the following VTF equation [29]:

$$\sigma(T) = \frac{A_\sigma}{\sqrt{T}} \exp\left(-\frac{B_\sigma}{T - T_{0\sigma}}\right), \quad (2)$$

where A_σ, B_σ, and $T_{0\sigma}$ are constants that are determined empirically. The ionic conductivity of the NaFSA-KFSA melt fitted well ($R^2 > 0.999$) to this VTF equation, with $A_\sigma = 1.02 \times 10^5$ mS cm^{-1} $K^{-1/2}$, $B_\sigma = 887$ K, and $T_{0\sigma} = 243$ K.

The relationship between ionic conductivity and molar conductivity is given by the following equation:

$$\lambda = \sigma \frac{M}{d}, \quad (3)$$

where λ is the molar conductivity, d is the density, and M is the average molecular weight of the melt. Fig. 3 shows the temperature dependence of the density for the eutectic NaFSA-KFSA melt. The density was measured as 2.14 g cm^{-3} at 363 K. The density linearly decreased with an increase in temperature, as expressed by the following equation:

$$d\ (\mathrm{g\ cm^{-3}}) = 2.43 - 8.08 \times 10^{-4} T \quad (4)$$

Fig. 4 shows plots of the logarithmic molar conductivity against the logarithmic reciprocal viscosity for the eutectic NaFSA-KFSA melt. If the viscosity and conductivity of the electrolyte obey Walden's rule, the product of the molar conductivity and viscosity is a constant [30]:

$$\lambda\eta = \text{const} \quad (5)$$

The interpretation of this equation is that the ionic conductivity of the liquid is governed by the viscosity. Although all of the plots (see Fig. 4) show a straight line, their gradients are slightly lower than unity. This tendency is called "decoupling" the behavior of ionic conductivity from that of viscosity [31,32]. Thus, in the case of a NaFSA-KFSA melt, the relationship between molar conductivity and viscosity should be described by the fractional Walden rule that is presented by the following equation [33]:

$$\lambda\eta^\alpha = \text{const}, \quad (6)$$

where α is a positive constant smaller than one and inversely proportional to the logarithm of the decoupling index, which indicates the level of decoupling [34]. For the NaFSA-KFSA melt, α was calculated to be 0.924, thus indicative of decoupling. The straight line, which has a unit gradient and passes through the points for 1 M KCl aqueous solution at 298 K, is called the "ideal" Walden line, as plotted as a dashed line in Fig. 4. The plot for the NaFSA-KFSA melt falls above the dashed line, thus indicating a "super ionic

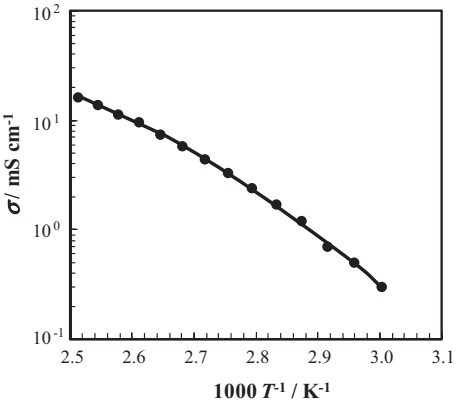

Fig. 2. Arrhenius plot of conductivity for a NaFSA-KFSA eutectic melt.

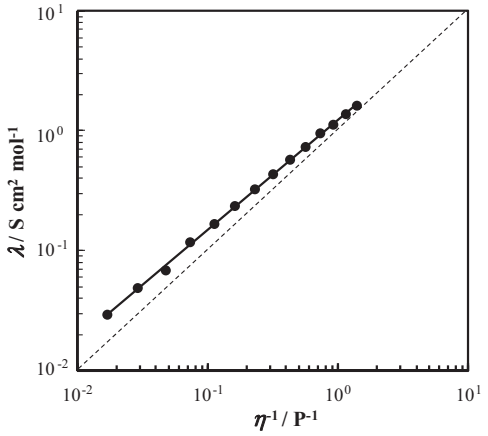

Fig. 4. Walden plot of molten NaFSA-KFSA.

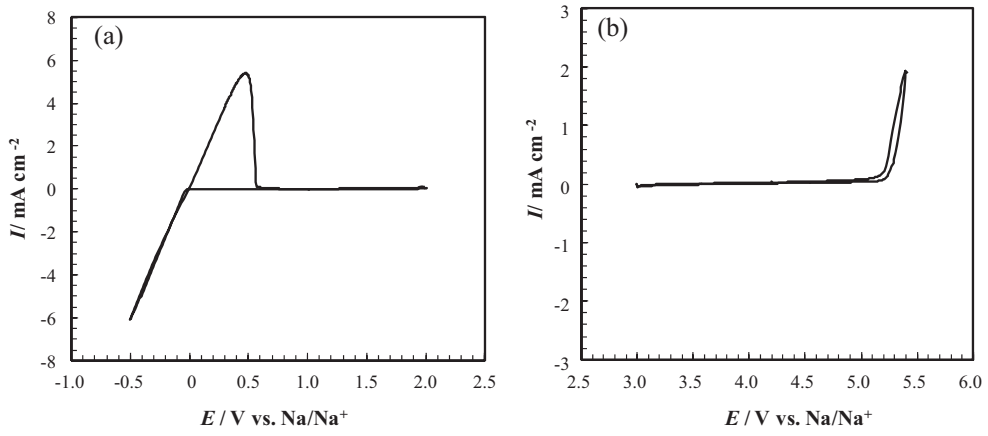

Fig. 5. Cyclic voltammograms of (a) a Cu plate electrode and (b) a glassy carbon rod electrode in NaFSA-KFSA eutectic melt at 363 K. Scan rate: 10 mV s^{-1}.

liquid area" where the ionic conductivity exhibits a higher value than that expected from the viscosity.

3.2. Electrochemical properties of the eutectic NaFSA-KFSA melt

Fig. 5 shows cyclic voltammograms of (a) copper and (b) a glassy carbon electrode in the NaFSA-KFSA melt at 363 K. A pair of cathodic and anodic currents is observed at 0 V vs. Na/Na^+ on a copper electrode. These cathodic and anodic currents are interpreted as the deposition of sodium metal and its dissolution, respectively. Galvanostatic electrolysis was performed at $-10\,mA\,cm^{-2}$ in order to identify the reaction at the cathode limit. As a result, deposits with partial metallic luster were obtained. When the deposits were analyzed by DSC, endothermic peaks were observed at the melting point of sodium metal, 371 K, as well as the melting point of the eutectic salt, 330 K. Hence, it was confirmed that only sodium metal was deposited at the cathode limit of NaFSA-KFSA. An anodic current was observed from around 5.2 V vs. Na/Na^+ on a glassy carbon electrode. This anodic current corresponds to the oxidation of FSA anion, though more studies are required to elucidate the detail of this reaction. The electrochemical window of NaFSA-KFSA melt is determined as 5.2 V at 363 K, with the limiting potentials defined as the potential at a current density of $0.1\,mA\,cm^{-2}$. Such a wide electrochemical window is highly desirable as an electrolyte for a battery because high voltage (i.e., high energy density) batteries can be constructed.

3.3. Charge–discharge tests of a Na/NaFSA-KFSA/$NaCrO_2$ cell

Before the charge–discharge experiments, the stability of aluminum, which was used as a current collector of the cathode, was checked by two methods. First, cyclic voltammetry was conducted for an aluminum plate electrode in the potential range of 1.0–5.0 V. Fig. 6 shows the measured voltammograms for the 1st, 2nd, and 5th cycles. The currents become smaller as the cycles proceed and are negligibly small in the potential range of 1.0–4.0 V, i.e., where the successive charge–discharge tests were conducted. The surface of the Al plate was partially discolored after the experiments. Second, the current on an aluminum plate electrode was measured during potentiostatic electrolysis at 4.5 V vs. Na/Na^+. As shown in Fig. 7, the current is negligibly small, below $0.1\,\mu A\,cm^{-2}$. Similar electrochemical stability of aluminum to that observed in LiTFSA-KTFSA-CsTFSA at 423 K [18] is explained by the formation of a passivation film on the aluminum surface. The passivation film is most probably formed by the reaction of Al^{3+} and FSA^-.

Fig. 8 shows charge–discharge curves for the 1st, 20th, and 100th cycle for a Na/NaFSA-KFSA/$NaCrO_2$ cell at the rate of 15 mA $(g\text{-}NaCrO_2)^{-1}$ at 353 K. The high and low cut-off voltages were 2.5 V and 3.5 V, respectively. Flat potential plateaus are repeatedly observed at approximately 3.0 V in both charge and discharge curves. The specific discharge capacity reached 77.3 mA h $(g\text{-}NaCrO_2)^{-1}$. Fig. 9 shows the cycling properties during the charge–discharge tests for 100 cycles. After the 50th cycle, the discharge capacity became almost constant and about 89% of the initial discharge capacity was maintained after 100 cycles. Except for the initial few cycles, the coulombic efficiency was higher than 99.9%. These results indicate that the electrolyte and electrode materials

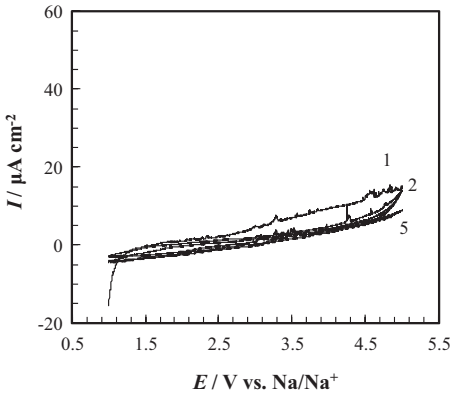

Fig. 6. Cyclic voltammograms of an Al plate electrode in NaFSA-KFSA eutectic melt at 363 K. Scan rate: 10 mV s^{-1}. Cycle number: 1, 2, and 5.

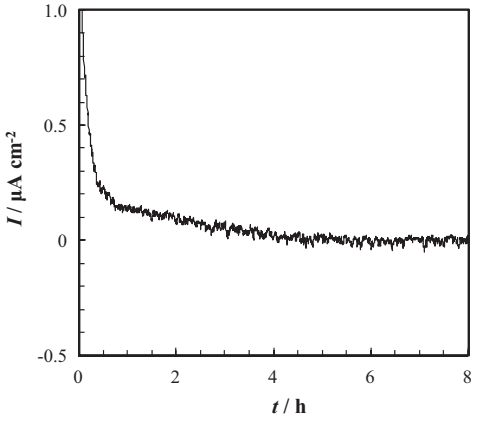

Fig. 7. A chronoamperogram of an Al plate electrode in NaFSA-KFSA eutectic melt at 363 K. Potential: 4.5 V vs. Na/Na^+.

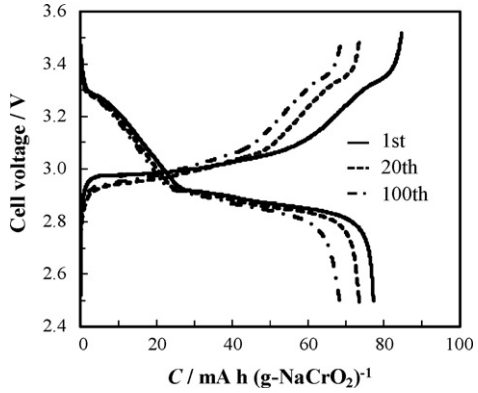

Fig. 8. Charge–discharge curves for a Na/NaFSA-KFSA/$NaCrO_2$ cell at 353 K. Charge–discharge rate: 15 mA g^{-1}. Cut-off voltage: 2.5–3.5 V. Cycle number: 1, 20, and 100.

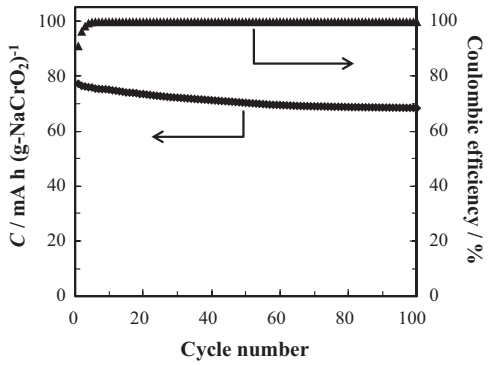

Fig. 9. Discharge capacity and coulombic efficiency for a Na/NaFSA-KFSA/$NaCrO_2$ cell at 353 K. Charge–discharge rate: 15 mA g^{-1}. Cut-off voltage: 2.5–3.5 V.

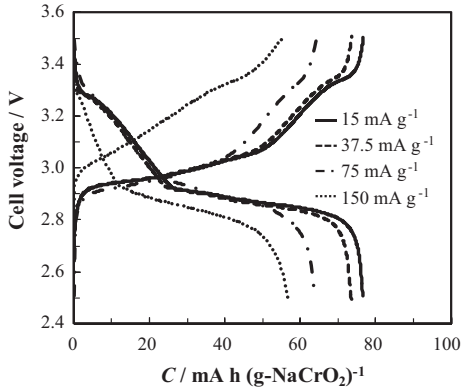

Fig. 10. Charge–discharge curves for a Na/NaFSA-KFSA/$NaCrO_2$ cell at 353 K. Charge–discharge rate: 150, 75, 37.5, 15 mA g^{-1}. Cut-off voltage: 2.5–3.5 V.

are stable at 353 K. Fig. 10 shows the charge–discharge curves at the rate of 15, 37.5, 75, and 150 mA (g-$NaCrO_2$)$^{-1}$. The shape of the curve did not change, even at the higher rates. This result indicates that no side reaction occurred during the cycles. It is concluded that the Na/NaFSA-KFSA/$NaCrO_2$ cell is highly promising as a new rechargeable sodium secondary battery operating at intermediate temperatures.

4. Conclusions

Densities, viscosities, ionic conductivities, and electrochemical windows have been measured for the eutectic NaFSA-KFSA melt. The viscosities and ionic conductivities are well described by VTF equations. The logarithmic molar conductivity is proportional to the logarithmic reciprocal viscosity and obeys the fractional Walden rule. The binary eutectic NaFSA-KFSA melt possesses a wide electrochemical window of ca. 5.2 V at 363 K. Aluminum is stable as the current collector material for the positive electrode, even at the high-potential region for this melt. A Na/NaFSA-KFSA/$NaCrO_2$ cell showed excellent cycle performance at 353 K, whereby 89% of the initial discharge capacity was maintained after 100 cycles with coulombic efficiencies of almost 100% at a charge–discharge rate of 15 mA (g-$NaCrO_2$)$^{-1}$. It is concluded that the binary eutectic NaFSA-KFSA melt is a promising electrolyte for a sodium secondary battery operating at intermediate temperatures, and that $NaCrO_2$ is a good candidate as a positive electrode active material.

Acknowledgement

This study was partly supported by Advanced Low Carbon Technology Research and Development Program (ALCA) of Japan Science and Technology Agency (JST).

References

[1] P.G. Bruce, B. Scrosati, J.-M. Tarascon, Angew. Chem. Int. Ed. 47 (2008) 2930–2946.
[2] J. Cabana, L. Monconduit, D. Larcher, M.R. Palacin, Adv. Mater. 22 (2010) E170–E192.
[3] B.L. Ellis, W.R.M. Mskahnouk, Y. Makimura, K. Toghill, L.F. Nazar, Nat. Mater. 6 (2007) 749–753.
[4] I.D. Gocheva, M. Nishijima, T. Doi, S. Okada, J. Yamaki, T. Nishida, J. Power Sources 187 (2009) 247–252.
[5] N. Recham, J.N. Chotard, L. Dupont, K. Djellab, M. Armand, J.M. Tarascon, J. Electrochem. Soc. 156 (2009) A993–A999.
[6] S. Komaba, T. Nakayama, A. Ogata, T. Shimizu, C. Takei, S. Takeda, A. Hokura, N. Nakai, ECS Trans. 16 (42) (2009) 43–55.
[7] S. Komaba, C. Takei, T. Nakayama, A. Ogata, N. Yabuuchi, Electrochem. Commun. 12 (2010) 355–358.
[8] Y. Yamada, T. Doi, I. Tanaka, S. Okada, J. Yamaki, J. Power Sources 196 (2011) 4837–4841.
[9] Y. Kawabe, N. Yabuuchi, M. Kajiyama, N. Fukuhara, T. Inamasu, R. Okuyama, I. Nakai, S. Komaba, Electrochem. Commun. 13 (2011) 1225–1228.
[10] S. Okada, S. Park, Electrochemistry 79 (2011) 470–476 (in Japanese).
[11] J.L. Sudworth, J. Power Sources 11 (1984) 143–154.
[12] T. Oshima, M. Kajita, A. Okuno, Int. J. Appl. Ceram. Technol. 1 (3) (2004) 269–276.
[13] J. Coetzer, J. Power Sources 18 (1986) 377–380.
[14] C.-H. Dustmann, J. Power Sources 127 (2004) 85–92.
[15] J.O'M. Bockris, A.K.N. Reddy, Modern Electrochemistry, vol. 1, Plenum Press, 1970 (Chapter 6, Ionic Liquids).
[16] K. Ui, M. Ueda, R. Hagiwara, Y. Mizuhata, Yoyuen oyobi Koon Kagaku 47 (2004) 114–123 (in Japanese).
[17] T. Nohira, T. Goto, R. Hagiwara, Yoyuen oyobi Koon Kagaku 50 (2008) 148–154 (in Japanese).
[18] A. Watarai, K. Kubota, M. Yamagata, T. Goto, T. Nohira, R. Hagiwara, K. Ui, N. Kumagai, J. Power Sources 183 (2008) 724–729.
[19] T. Nohira, T. Ishibashi, R. Hagiwara, J. Power Sources 205 (2012) 506–509.
[20] R. Hagiwara, T. Nohira, A. Fukunaga, S. Sakai, K. Nitta, S. Inazawa, Electrochemistry 80 (2012) 98–103 (in Japanse).
[21] R. Hagiwara, K. Tamaki, K. Kubota, T. Goto, T. Nohira, J. Chem. Eng. Data 53 (2008) 355–358.
[22] K. Kubota, T. Nohira, T. Goto, R. Hagiwara, J. Chem. Eng. Data 53 (2008) 2144–2147.
[23] K. Kubota, K. Tamaki, T. Nohira, T. Goto, R. Hagiwara, Electrochim. Acta 55 (2010) 1113–1119.
[24] K. Kubota, T. Nohira, T. Goto, R. Hagiwara, Electrochem. Commun. 10 (2008) 1886–1888.
[25] K. Kubota, T. Nohira, T. Goto, R. Hagiwara, ECS Trans. 16 (24) (2009) 91–98.
[26] K. Kubota, T. Nohira, R. Hagiwara, J. Chem. Eng. Data 55 (2010) 3142–3146.
[27] K. Kubota, T. Nohira, R. Hagiwara, Electrochim. Acta 66 (2012) 320–324.
[28] A.J. Easteal, C.A. Angell, J. Chem. Phys. 56 (1972) 4231–4233.
[29] C.A. Angell, J. Phys. Chem. 68 (1964) 1917–1929.
[30] P. Walden, Z. Phys. Chem. 55 (1906) 207–249.
[31] C.A. Angell, W. Xu, M. Yoshizawa, A. Hayashi, J.P. Belieres, in: H. Ohno (Ed.), Ionic Liquids: The Front and Future of Material Development, High Technology Information, Tokyo, 2003, p. 43 (in Japanese).
[32] C.A. Angell, M. Wu Xu, A. Yoshizawa, J.-P. Hayashi, P. Belieres, M. Lucas, H. Videa, in: Ohno (Ed.), Electrochemical Aspects of Ionic Liquids, Wiley Interscience, 2005 (Chapter 2).
[33] W. Xu, C.A. Angell, Science 302 (2003) 422–425.
[34] M. Videa, C.A. Angell, J. Phys. Chem. B 103 (1999) 4185–4190.